Proposal for Direct Measurement of Topological Invariants in Optical Lattices

Lei Wang,[1,2] Alexey A. Soluyanov,[1] and Matthias Troyer[1]
[1]*Theoretische Physik, ETH Zurich, 8093 Zurich, Switzerland*
[2]*Beijing National Lab for Condensed Matter Physics and Institute of Physics, Chinese Academy of Sciences, Beijing 100190, China*
(Received 5 March 2013; published 19 April 2013)

We propose an experimental technique for classifying the topology of band structures realized in optical lattices, based on a generalization of topological charge pumping in quantum Hall systems to cold atoms in optical lattices. Time-of-flight measurement along one spatial direction combined with *in situ* detection along the transverse direction provides a direct measure of the system's Chern number, as we illustrate by calculations for the Hofstadter lattice. Based on an analogy with Wannier function techniques of topological band theory, the method is very general and also allows the measurement of other topological invariants, such as the $\mathbb{Z}_2$ topological invariant of time-reversal symmetric insulators.

DOI: 10.1103/PhysRevLett.110.166802 PACS numbers: 67.85.−d, 03.65.Vf

Recent advances in experimental techniques have led to realization of synthetic gauge fields [1–5] and spin-orbit coupling [6,7] in cold atomic gases. These new developments allow one to study a variety of topological phases of condensed matter physics by using cold gases of neutral atoms trapped in optical lattices. Such topological phases occur in systems whose Hilbert space has a nontrivial topological structure, and they are classified according to the value of a corresponding quantum number, the topological invariant.

Particular examples of such phases in condensed matter include the quantum Hall insulators [8] or the quantum anomalous Hall insulators [9], where the topological invariant of the Hilbert space is the so-called Chern number [10]. Some recent experiments [3–5,11] point towards the possibility of realizing an optical lattice with a nonzero Chern number in the near future.

Once the desired lattice is created, the question of experimental verification of the nontrivial topology arises. Unlike condensed matter systems, where a routine measurement of the Hall conductance reveals the Chern number value [8], cold atom systems require a special setup [12] for transport measurements. Edge state probes of condensed matter experiments also become cumbersome in a cold atom environment, since the smooth harmonic potential washes out the edge states associated with the quantum Hall state. This problem can potentially be circumvented by enhancing a weak Bragg signal from the topological edge states by means of specifically tuned Raman transitions [13,14]. Other approaches, which do not have an immediate analogy among solid state experiments, might also allow for the measurement of Chern numbers in optical lattices [15–19]. However, the quest for a universal method to obtain Chern numbers and other topological invariants directly in a single measurement, avoiding a sophisticated experimental setup or data analysis, remains open.

In this Letter, we tackle the problem of detecting topological invariants in optical lattice systems from a very different perspective, drawing an analogy to the theory of electric polarization of crystalline solids [20] to suggest a simple and effective method to measure Chern numbers in cold atom systems. We introduce the concept of hybrid time-of-flight (HTOF) images, referring to an *in situ* measurement of the cloud's density in one direction during free expansion in the other. The HTOF reveals the topology of the optical lattice just as hybrid Wannier functions (HWFs) do in band theory [21,22]. We illustrate our approach by numerical simulations of a square optical lattice that realizes a Hofstadter model [23] and discuss how it works in lattices with a more complicated geometry. Our method does not require the presence of the sharp edge states and is not affected by a soft harmonic trap. It can also be used to detect the $\mathbb{Z}_2$ topological invariant of time-reversal ($\mathcal{T}$) symmetric topological insulators.

The modern theory of electric polarization of crystalline solids [20,24] relates the electronic polarization P to the geometry of the underlying band structure. For a 1D insulator with a single occupied band $P = \frac{1}{2\pi} \oint_{BZ} \mathcal{A}(k)dk$, where k is the crystal momentum, $\mathcal{A}(k) = i\langle u_k|\partial_k|u_k\rangle$ is the Berry connection [25], and the u's are the lattice-periodic parts of the Bloch functions. Alternatively, we will use the fact that the polarization can be written [20] as the center of mass of the Wannier function constructed for the occupied band [26], which can be defined as an expectation value of the position operator projected onto the occupied state [27,28].

In two dimensions (2D) an insulating Hamiltonian can be viewed as a fictitious 1D insulator subject to an external parameter k_x. Polarization of this 1D insulator can be defined by means of HWFs [29], which are localized in only one direction retaining Bloch character in the other. The polarization at each k_x is given by the center of mass of the corresponding HWF [22].

The definitions of electronic polarization given above are gauge dependent, meaning that P is defined only modulo a lattice vector. For measurements, one has to consider the change in polarization induced by a change

 © 2013 American Physical Society

in an external parameter [20]. In the 2D insulator considered above, k_x plays the role of such a parameter. When k_x is adiabatically changed by 2π, the change in polarization, i.e., the shift of the HWF center, is proportional to the Chern number [20]. This is a manifestation of topological charge pumping [30,31], with k_x being the adiabatic pumping parameter.

A generalization of these ideas to cold atomic gases is a natural way to measure the Chern number in optical lattices. We replace the HWFs of band theory with hybrid densities $\rho(k_x, y)$, which are the particle densities resolved along the y direction as a function of k_x. Note that, while for an extended system the HWF charge center position cannot be reconstructed from the single particle density [24], this becomes possible in a finite system where the position operator is well defined [32]. Hence in a system with finite extent L_y in the y direction we can calculate the HWF center as

$$\bar{y}(k_x) = \frac{\int_0^{L_y} y\rho(k_x, y)dy}{\int_0^{L_y} \rho(k_x, y)dy}. \quad (1)$$

The proportionality between the shift of the HWF center and the Chern number still holds in the open system. The Chern number measures the charge transported from one boundary to the other as k_x is cycled by 2π. An experimental measurement of the shift in the hybrid density will hence directly determine the Chern number.

Experimentally, $\rho(k_x, y)$ is measured by an HTOF measurement, in which the lattice and trap are switched off along the x direction while keeping the lattice and harmonic confinement unchanged in the y direction. In the long time limit [33] TOF images map out the crystal momentum distribution along k_x [34]. At the same time, the system is still confined in the y direction, and a real-space density resolution can be done.

We now show HTOF unambiguously determine the Chern number by performing a numerical simulation of the Hofstadter model [23] on a square lattice. Its Hamiltonian is given by

$$H_{\text{lattice}} = -J_x \sum_{m,n} e^{i2\pi n\Phi} c^\dagger_{m+1,n} c_{m,n} - J_y \sum_{m,n} c^\dagger_{m,n+1} c_{m,n} + \text{H.c.}, \quad (2)$$

where J_α is the hopping amplitude in the $\alpha = \{x, y\}$ direction and $c_{m,n}$ is the fermionic annihilation operator, with m and n being the column and row indices of the lattice, respectively (see Fig. 1).

An atom hopping clockwise around a plaquette accumulates a phase Φ. We consider $\Phi = p/q$, where p and q are two relatively prime integers. The hopping matrix elements $J_x e^{i2\pi n\Phi}$ along the x direction depend on the row index n so that each unit cell contains q sites. In the following, we fix $q = 7$ and assume that only the lowest band is occupied. The Chern number C of the lowest band

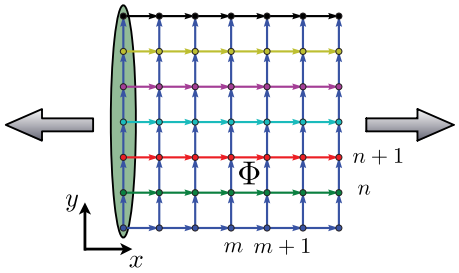

FIG. 1 (color online). Square lattice illustrating the Hofstadter model of Eq. (2). The oval marks $q = 7$ sites of the unit cell. Small arrows indicate the directions in which the phase of the hopping amplitude is chosen to be positive. Different colors of these arrows correspond to different values of the phase. Large arrows indicate the direction of the free expansion of the atomic cloud in HTOF images.

is determined by the Diophantine equation $1 = qs + pC$ [10,35,36], where s is an integer and $|C| \leq q/2$.

We first consider an infinite ribbon of this model with width $L_y = 10$, setting $J_x = J_y = J$ and $p = 1$, which corresponds to a Chern number $C = 1$. In the spectrum shown in Fig. 2(a), we see that, as expected for $p = 1$, two edge states cross the Fermi level. Analogously to the 2D insulator considered above, this setup can be viewed as a finite 1D chain subject to a k_x-driven pump. From this point of view, the hybrid density $\rho(k_x, n)$ describes the change in the density of the 1D system as a function of the pumping parameter. Figure 2(b) shows that the hybrid density is shifted by one unit cell in the bulk, indicating that a single charge is pumped across the system, as expected for $C = 1$.

We calculate the k_x dependence of the HWF center by taking a tight-binding limit of Eq. (1):

$$\bar{n}(k_x) = \frac{\sum_n n\rho(k_x, n)}{\sum_n \rho(k_x, n)}. \quad (3)$$

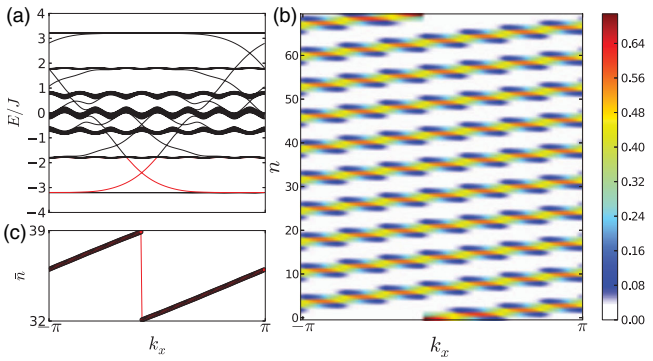

FIG. 2 (color online). Results for a ribbon ($L_y = 10$) of the Hofstadter lattice model with $p/q = 1/7$ and corresponding Chern number $C = 1$. (a) Energy spectrum: two edge states (in red) cross the bulk energy gap. (b) Hybrid density $\rho(k_x, n)$ shifts by one unit cell in a 2π cycle. (c) The center of mass of the hybrid density Eq. (3) jumps by one unit cell.

As shown in Fig. 2(c), $\bar{n}(k_x)$ jumps by one unit cell ($q = 7$ sites), analogous to the HWF shift in Chern insulators [21].

Having established a clear connection between the hybrid density and Chern number, we now turn to a more realistic case by adding a harmonic trapping potential of the form

$$H_{\text{trap}} = V_{\text{T}} \sum_{m,n} [(m - L_x/2)^2 + (n - qL_y/2)^2] c^{\dagger}_{m,n} c_{m,n}, \tag{4}$$

where $L_{x(y)}$ denotes the number of unit cells in the $x(y)$ direction. The system contains qL_y rows and L_x columns. The values of V_{T} and the number of atoms $N = 300$ are chosen such that the atom cloud has a large insulating region corresponding to $1/q$ filling at the trap center. We now consider the cases $p = 1$ and $p = 3$, corresponding to Chern numbers $+1$ and -2, respectively.

There is no significant difference in the real space densities of the two states, since the harmonic trap smears out the edge states [13]. In contrast, the HTOF density profiles allow one to directly read off the Chern numbers. We calculate these HTOF images by first solving the Schrödinger equation $(H_{\text{lattice}} + H_{\text{trap}})\psi_i(m, n) = \varepsilon_i \psi_i(m, n)$ and constructing HWFs by means of the Fourier transform in the x direction:

$$\psi_i(k_x, n) = \sum_{m=0}^{L_x - 1} e^{ik_x m} \psi_i(m, n). \tag{5}$$

We then use these wave functions to construct the hybrid particle density of the HTOF measurement:

$$\rho(k_x, n) = \frac{1}{N} \sum_{i=1}^{N} |\psi_i(k_x, n)|^2. \tag{6}$$

HTOF images obtained in this way are shown in Fig. 3 and clearly exhibit the topological charge pumping effect despite the presence of a trap: The hybrid density shifts by C unit cells along the y direction as k_x changes from $-\pi$ to π. Thus, the hybrid density is an accurate probe of topological properties and allows one to directly measure the Chern number.

To get deeper understanding, we consider the case of vanishing transverse coupling $J_y = 0$, corresponding to a set of decoupled tight-binding chains with dispersions $\epsilon_n(k_x) = -2J_x \cos(k_x - 2\pi np/q)$. The position of the band minimum shifts by $2\pi p/q$ from one chain to the next, as shown in Fig. 4(a) for $p = 3$. If an infinitesimal coupling J_y is added, the 2D lattice is in the Chern insulating regime. Charge pumping can be inferred by tracing the change in the position of the valence band minima for weakly coupled chains: Connecting nearest neighbor points in Fig. 4(a) reveals a shift by two unit cells ($|C| = 2$) in the course of a 2π change of momentum [dashed red arrow in Fig. 4(a)]. This illustrates the geometrical interpretation of the Diophantine equation [10], as also discussed in Ref. [37] in a different context.

The above analysis allows for an alternative way of describing the HTOF results presented in Figs. 3(a) and 3(b). We introduce sublattice densities $\rho^a(k_x, \tilde{n})$, which correspond to the particle density on the ath site of the $\tilde{n}$th unit cell. These sublattice densities, shown in Fig. 4(b), shift along the y direction as k_x changes, illustrating the motion of charge. The motion of charge can also be tracked in the total sublattice density obtained by summing $\rho^a(k_x, \tilde{n})$ over the unit cells:

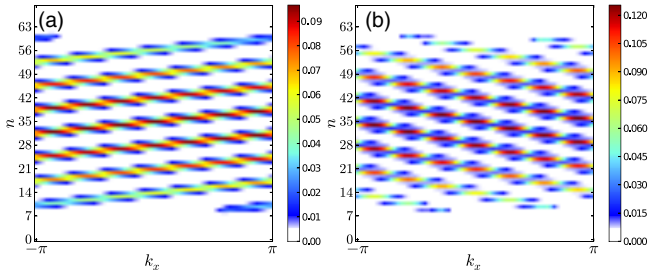

FIG. 3 (color online). The HTOF images for the Hofstadter lattice ($L_x = 70$, $L_y = 10$, $N = 300$) in the presence of the harmonic trap: (a) for $p/q = 1/7$ with $C = 1$ ($V_T = 0.001$) and (b) for $p/q = 3/7$ with $C = -2$ ($V_T = 0.001$). Chern numbers can be determined as the number of unit cells traversed by the hybrid density in the course of a 2π cycle. Upward (downward) direction of the shift corresponds to a positive (negative) Chern number. The broadening of lines corresponds to exponential localization of the peaks of the hybrid density.

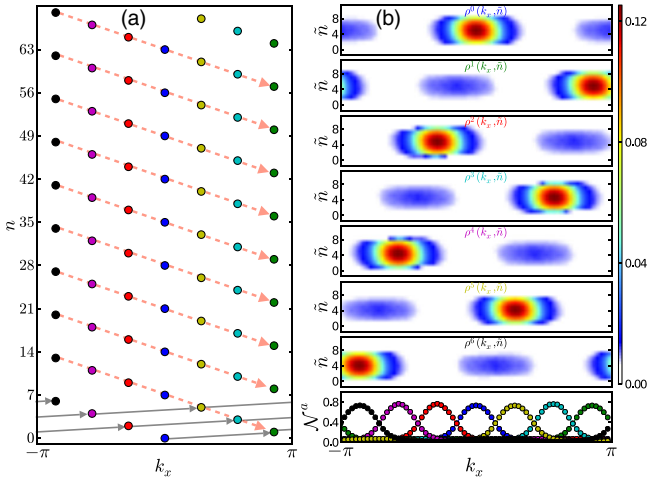

FIG. 4 (color online). (a) Valence band minima of decoupled ($J_y = 0$) 1D chains of the Hofstadter model with $p/q = 3/7$. Different colors correspond to different sublattice chains. Solid gray arrows indicate the shift in the dispersion due to the phase factors. Dashed red arrows connect nearest neighbor points and illustrate charge pumping. (b) The sublattice densities $\rho^a(k_x, \tilde{n})$ within a unit cell and the total sublattice density $\mathcal{N}^a(k_x)$ for different values of a. The color scheme is the same as in the left panel, and the model parameters are the same as in Fig. 3(b).

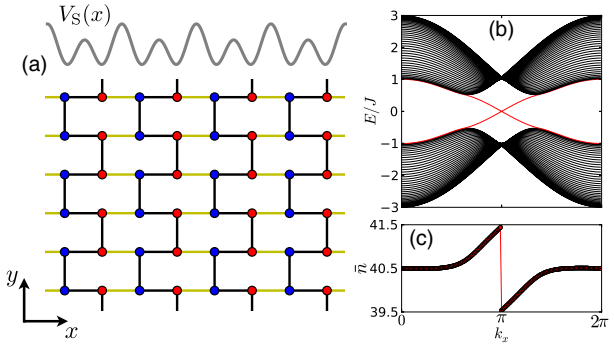

FIG. 5 (color online). (a) The brick-wall lattice split into 1D chains. Thick (black) and light (yellow) bonds indicate intra- and interchain hoppings, respectively. The shape of an imposed superlattice potential $V_S(x)$ is shown schematically (in gray). (b) Energy spectrum of a Haldane model in the ribbon geometry. Edge states are shown in red. (c) The shift of the center of mass of the hybrid density indicates a nontrivial Chern number ($C = 1$).

$$\mathcal{N}^a(k_x) = \sum_{\tilde{n}=0}^{L_y-1} \rho^a(k_x, \tilde{n}). \tag{7}$$

Thus, the topological nature of the state can also be seen in the total sublattice density, which is potentially accessible in a TOF experiment that can distinguish different sublattices [3,38]. However, such an analysis is specific to the Hofstadter model, while the HTOF measurement is generally applicable.

The square lattice considered so far is particularly simple, since a straightforward partition into 1D chains is possible. HTOF measurement can also work for other lattice geometries such as the honeycomb lattice, which is topologically equivalent to the brick-wall lattice shown in Fig. 5(a). Such a lattice was used to create Dirac points in optical lattices [11]. This lattice is a potential candidate for realizing the Haldane model [9], which is a canonical example of a Chern insulator.

A partition of the brick-wall lattice into 1D chains, along which the charge is pumped, is illustrated in Fig. 5(a) with solid dark bonds. The chains consist of two sublattices offset from each other in the x direction. Due to this offset, the charge pumping is not directly visible in the HTOF image unless one separately measures them for each sublattice (for example, by using the superlattice technique of Ref. [38]). As illustrated in Fig. 5(c), the center of mass of the hybrid density along the zigzag 1D chain is indeed shifted by one unit cell along the 1D chain, revealing the Chern number $C = 1$ of the Haldane model.

The HTOF technique can determine not only Chern numbers, but also the $\mathbb{Z}_2$ topological invariant of $\mathcal{T}$-symmetric insulators [39]. In band theory this invariant can be obtained by means of HWFs [40–42], once they form $\mathcal{T}$ images of one another. The occupied single particle states of the insulator can always be split into two sets of states (related by $\mathcal{T}$ symmetry) where each set has a well-defined Chern number [43]. For a wide range of models, such a splitting can be achieved by projecting the occupied states onto particular spin directions [44,45]. If the values of thus obtained spin Chern numbers are odd, the system is in the $\mathbb{Z}_2$-insulating regime. In the context of cold atoms, considering a minimal model with only two occupied bands, a spin-projected HTOF measurement of spin-resolved densities would serve as a direct measurement of the spin Chern numbers and, hence, of the $\mathbb{Z}_2$ invariant.

The proposed HTOF technique is not only practical, providing exhaustive information about the topological state of an optical lattice, but is also a conceptually novel idea for using a cold atom lattice as a quantum simulator. Hybrid density measurement as proposed here for cold atom systems is not possible in condensed matter experiments, and the HWFs are used only in computer simulations. These experiments can thus access novel probes of topological order and will give rise to further implementations of so far numerical experiments of condensed matter in real experiments on cold atom systems.

We thank David Vanderbilt, Thomas Uehlinger, Daniel Greif, and Gregor Jotzu for helpful discussions. The work was supported by the Swiss National Science Foundation through the NCCR QSIT and the European Research Council. Simulations were run on the Brutus cluster at ETH Zurich.

[1] Y. J. Lin, R. L. Compton, K. Jiménez-García, J. V. Porto, and I. B. Spielman, Nature (London) **462**, 628 (2009).
[2] Y.-J. Lin, R. L. Compton, K. Jimenez-Garcia, W. D. Phillips, J. V. Porto, and I. B. Spielman, Nat. Phys. **7**, 531 (2011).
[3] M. Aidelsburger, M. Atala, S. Nascimbène, S. Trotzky, Y. Chen, and I. Bloch, Phys. Rev. Lett. **107**, 255301 (2011).
[4] K. Jimenez-Garcia, L. LeBlanc, R. Williams, M. Beeler, A. Perry, and I. Spielman, Phys. Rev. Lett. **108**, 225303 (2012).
[5] J. Struck, C. Ölschläger, M. Weinberg, P. Hauke, J. Simonet, A. Eckardt, M. Lewenstein, K. Sengstock, and P. Windpassinger, Phys. Rev. Lett. **108**, 225304 (2012).
[6] P. Wang, Z.-Q. Yu, Z. Fu, J. Miao, L. Huang, S. Chai, H. Zhai, and J. Zhang, Phys. Rev. Lett. **109**, 095301 (2012).
[7] L. W. Cheuk, A. T. Sommer, Z. Hadzibabic, T. Yefsah, W. S. Bakr, and M. W. Zwierlein, Phys. Rev. Lett. **109**, 095302 (2012).
[8] K. Klitzing, G. Dorda, and M. Pepper, Phys. Rev. Lett. **45**, 494 (1980).
[9] F. D. M. Haldane, Phys. Rev. Lett. **61**, 2015 (1988).
[10] D. J. Thouless, M. Kohmoto, M. P. Nightingale, and M. denijs, Phys. Rev. Lett. **49**, 405 (1982).
[11] L. Tarruell, D. Greif, T. Uehlinger, G. Jotzu, and T. Esslinger, Nature (London) **483**, 302 (2012).
[12] J.-P. Brantut, J. Meineke, D. Stadler, S. Krinner, and T. Esslinger, Science **337**, 1069 (2012).

[13] M. Buchhold, D. Cocks, and W. Hofstetter, Phys. Rev. A **85**, 063614 (2012).
[14] N. Goldman, J. Beugnon, and F. Gerbier, Phys. Rev. Lett. **108**, 255303 (2012).
[15] E. Alba, X. Fernandez-Gonzalvo, J. Mur-Petit, J. Pachos, and J. Garcia-Ripoll, Phys. Rev. Lett. **107**, 235301 (2011).
[16] E. Zhao, N. Bray-Ali, C. Williams, I. Spielman, and I. Satija, Phys. Rev. A **84**, 063629 (2011).
[17] M. Atala, M. Aidelsburger, J. T. Barreiro, D. Abanin, T. Kitagawa, E. Demler, and I. Bloch, arXiv:1212.0572.
[18] D. A. Abanin, T. Kitagawa, I. Bloch, and E. Demler, arXiv:1212.0562v1.
[19] N. Goldman, J. Dalibard, A. Dauphin, F. Gerbier, M. Lewenstein, P. Zoller, and I. B. Spielman, arXiv:1212.5093v1.
[20] R. D. King-Smith and D. Vanderbilt, Phys. Rev. B **47**, 1651 (1993).
[21] S. Coh and D. Vanderbilt, Phys. Rev. Lett. **102**, 107603 (2009).
[22] N. Marzari, A. Mostofi, J. R. Yates, I. Souza, and D. Vanderbilt, Rev. Mod. Phys. **84**, 1419 (2012).
[23] D. Hofstadter, Phys. Rev. B **14**, 2239 (1976).
[24] R. Resta, Rev. Mod. Phys. **66**, 899 (1994).
[25] M. V. Berry, Proc. R. Soc. A **392**, 45 (1984).
[26] W. Kohn, Phys. Rev. **115**, 809 (1959).
[27] S. A. Kivelson, Phys. Rev. B **26**, 4269 (1982).
[28] N. Marzari and D. Vanderbilt, Phys. Rev. B **56**, 12 847 (1997).
[29] C. Sgiarovello, M. Peressi, and R. Resta, Phys. Rev. B **64**, 115202 (2001).
[30] D. J. Thouless, Phys. Rev. B **27**, 6083 (1983).
[31] Q. Niu, Phys. Rev. Lett. **64**, 1812 (1990).
[32] R. Resta, Phys. Rev. Lett. **80**, 1800 (1998).
[33] F. Gerbier, S. Trotzky, S. Fölling, U. Schnorrberger, J. Thompson, A. Widera, I. F. Bloch, L. Pollet, M. Troyer, B. Capogrosso-Sansone, N. Prokof'ev, and B. Svistunov, Phys. Rev. Lett. **101**, 155303 (2008).
[34] Due to the short coherence length of the band insulator, the Fresnel interference term [33] can safely be ignored for typical expansion times. For example, with ^{40}K atoms in a typical optical lattice at expansion times of $\sim$10 ms will suffice.
[35] M. Kohmoto, Phys. Rev. B **39**, 11 943 (1989).
[36] I. Dana, Y. Avron, and J. Zak, J. Phys. C **18**, L679 (1985).
[37] Z. Huang and D. Arovas, Phys. Rev. B **86**, 245109 (2012).
[38] S. Fölling, S. Trotzky, P. Cheinet, M. Feld, R. Saers, A. Widera, T. Müller, and I. F. Bloch, Nature (London) **448**, 1029 (2007).
[39] M. Z. Hasan and C. L. Kane, Rev. Mod. Phys. **82**, 3045 (2010).
[40] L. Fu and C. L. Kane, Phys. Rev. B **74**, 195312 (2006).
[41] A. A. Soluyanov and D. Vanderbilt, Phys. Rev. B **83**, 235401 (2011).
[42] R. Yu, X.-L. Qi, A. Bernevig, Z. Fang, and X. Dai, Phys. Rev. B **84**, 075119 (2011).
[43] A. Soluyanov and D. Vanderbilt, Phys. Rev. B **85**, 115415 (2012).
[44] D. Sheng, Z.-Y. Weng, L. Sheng, and F. D. M. Haldane, Phys. Rev. Lett. **97**, 036808 (2006).
[45] E. Prodan, Phys. Rev. B **80**, 125327 (2009).